JOURNAL OF CATALYSIS **178,** 108–118 (1998)
ARTICLE NO. CA982124

Catalyst Transformation during NO + NH_3 Reaction over Vanadium Oxide Using *in Situ* FTIR Emission Spectroscopy

D. H. Sullivan,[1] M. P. Harold,[2] and W. C. Conner, Jr.

Department of Chemical Engineering, University of Massachusetts, Amherst, Massachusetts 01003

Received October 31, 1997; revised March 17, 1998; accepted April 27, 1998

The low-frequency capabilities of infrared emission spectroscopy (IRES) were exploited to examine the reduction of vanadium pentoxide (V_2O_5) by ammonia and hydrogen, and the reoxidation of reduced vanadia by oxygen. The catalytic reduction of NO with NH_3 over V_2O_5 powder in the absence of O_2 was also investigated with IRES. The reduction of V_2O_5 was found to occur stepwise ($V^{5+} \rightarrow V^{4+} \rightarrow V^{3+}$), with the rate being controlled by the diffusion of oxygen through the crystal lattice. Vanadia reduction occurred even in high NO/NH_3 atmospheres, although the presence of NO did effect the rate of reduction. © 1998 Academic Press

INTRODUCTION

Metal oxide catalysts are employed in many oxidation and reduction processes during which the catalyst is sequentially oxidized and reduced. Furthermore, under some conditions net changes in the structure and in the metal valance state of a metal–oxide catalyst can occur during a catalytic oxidation/reduction process. These changes may in turn have a profound effect on the catalytic properties of the oxide. Knowledge of the interaction of reducing and oxidizing reactants with the metal oxide and the redox processes which result is key to the complete understanding of the catalytic mechanism.

Characterization of Metal Valance State of Metal Oxides

Several techniques have been employed to study the role of redox processes in catalytic reactions. Centi *et al.* (1) studied the oxidation of *n*-butane to maleic anhydride over a vanadium–phosphorous–oxide (VPO) catalyst with a varying hydrocarbon-to-oxygen feed ratio. Using a variety of *ex situ* analyses to characterize the oxidation state, including wet chemical analysis, electron paramagnetic resonance (EPR) and diffuse-reflectance spectrophotometry, they were able to correlate the selectivity to butenes, and partial oxidation products other than maleic anhydride to the reduction of vanadium atoms from V^{5+} and V^{4+} to V^{3+} at a high butane-to-oxygen ratio. The authors proposed a mechanism involving two redox cycles: (i) a V^4–V^3 cycle in the oxidation of *n*-butane to olefins and (ii) a V^5–V^4 cycle in the oxidation of olefins to maleic anhydride.

Similarly, Lunsford (2) used EPR to study the mechanism of the NO–NH_3 reaction over a Cu–Y zeolite catalyst and found that the rate of N_2 formation dropped along with the Cu^{2+} EPR signal at elevated temperature. The selective reduction of NO to N_2 was proposed to occur on Cu^{2+} sites, while a slow reduction of Cu^{2+} results in the deactivation of the catalyst.

Bielanski *et al.* (3) have shown that the vanadia reduction rate is limited by solid-state lattice diffusion, and the vanadium reduces stepwise, i.e., $V^{5+} \rightarrow V^{4+} \rightarrow V^{3+}$ using *ex situ* EPR and wet chemical analysis.

Each of the techniques used in these studies requires *ex situ* analysis. Furthermore, EPR (as employed by Bielanski *et al.* (3) can only detect paramagnetic species such as V^{4+}, but not V^{5+} or V^{3+}. In a previous paper (4), we demonstrated the ability of IRES to record *in situ* spectra of the metal–oxygen stretching region (<1000 cm^{-1}). It was suggested that changes in the oxidation state of metal oxide catalysts could be correlated to changes in this region of the IR spectra. Furthermore, infrared emission spectroscopy (IRES) provides a near-surface measure of the oxidation state of the sample.

Radiation which is emitted from a point within a solid must transmit through the bulk of the solid. Some of this radiation is absorbed. The maximum depth of the solid from which emitted radiation can be detected is $\sim 5/\alpha$, where α is the absorbtivity of the solid. Less than 1% of the radiant flux can transmit through this distance. The absorbtivity is defined by

$$\alpha = 4\pi n_I \bar{\nu}, \qquad [1]$$

where $\bar{n}$ is the wave number (the reciprocal of wavelength) of the radiation, and n_I is the imaginary part of the complex refractive index (5). Assuming $n_I \sim 1$, a conservative estimate for the maximum depth of penetration for IR radiation at 1,000 cm^{-1} is 4 μm.

[1] Present address: Union Camp Technology Center, P.O. Box 3301, Princeton, NJ 08543.

[2] Present address: Dupont Experimental Station, Central Research and Development, Wilmington, DE 19880-0304.

0021-9517/98 $25.00

NO Reduction by NH_3 over Vanadia Catalysts

Nitric oxides (primarily NO and NO_2) are an important class of air pollutants which result largely from the reaction of N_2 with O_2 in high-temperature combustion processes. The selective catalytic reduction (SCR) process has become the dominant NO_x abatement technique used in power generation plants which contribute nearly half of U.S. NO_x emissions (6). This dominance is primarily due to the high NO_x conversion which can be achieved with SCR (6–8). The process involves the selective reduction of NO by NH_3 in the presence of O_2 over a catalyst. The most popular commercial catalyst is vanadia supported on titania, due to its high activity at low temperature and resistance to poisoning by SO_2 (7).

The NO–NH_3 reaction, in the absence of O_2, can be described by two reactions which produce N_2 and N_2O, respectively:

$$6\,NO + 4\,NH_3 \rightarrow 5\,N_2 + 6\,H_2O \quad [2]$$

$$8\,NO + 2\,NH_3 \rightarrow 5\,N_2O + 3\,H_2O. \quad [3]$$

In the presence of O_2, oxidation of NH_3 can also occur as follows:

$$4\,NH_3 + 3\,O_2 \rightarrow 2\,N_2 + 6\,H_2O \quad [4]$$

$$2\,NH_3 + 2\,O_2 \rightarrow N_2O + 3\,H_2O \quad [5]$$

$$4\,NH_3 + 5\,O_2 \rightarrow 4\,NO + 6\,H_2O. \quad [6]$$

Miyamoto and co-workers (9–13) proposed an Eley–Rideal mechanism (Fig. 1) to explain the kinetic behavior of the reaction in the presence of O_2 over vanadia catalysts under dilute, commercial conditions (<1000 ppm NO and NH_3). They found that negligible N_2 was produced when the catalyst was treated with NO and O_2 at 250°C and subsequently exposed to NH_3. However, significant amounts

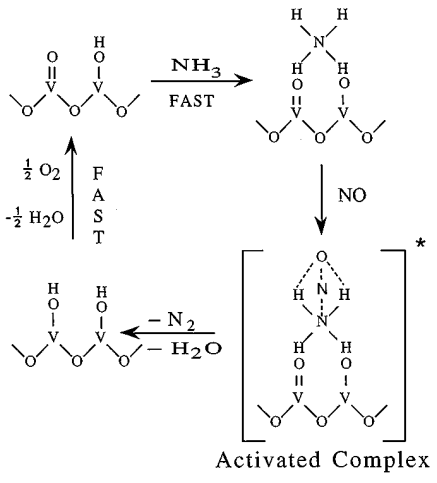

FIG. 1. Eley–Rideal mechanism for NO–NH_3 reaction in the presence of O_2 on V_2O_5 (after Miyamoto (12)).

of N_2 and water were produced when the catalyst was treated with NH_3 and subsequently exposed to gaseous NO at 100°C and higher. Furthermore, the reaction was found to be first-order with respect to NO and zero-order with respect to NH_3. They proposed that NH_3 adsorbed strongly (as NH_4^+) (14) while NO adsorbed very little or not at all on a fully oxidized V_2O_5 surface (15). Instead gaseous NO reacted with adsorbed NH_3 to produce N_2 and H_2O. In the process, the vanadia is reduced by hydrogen atoms from NH_3 decomposition (16). Gaseous O_2, or to a lesser extent NO, can reoxidize the vanadia to complete the redox cycle.

A key point of this mechanism is the role of O_2. Miyamoto claimed that the reaction involved a redox cycle where lattice oxygen was incorporated into the reaction products, thus leaving an oxygen vacancy on the surface which could be reoxidized by O_2. Miyamoto proposed that reduction takes place at the terminal oxygen sites on the basal planes of vanadia (Fig. 1); however, this point has been disputed (17, 18). The key conclusion was that O_2 was not necessary for the NO–NH_3 reaction directly, rather its role was to maintain the oxidation state of the vanadium. Miyamoto points out that lattice O atoms in the subsurface layer of the catalyst can also reoxidize the surface in the absence of (or at low levels of) gaseous O_2. Inomata *et al.* (10) confirmed this role by showing that low levels of O_2 increased the reaction rate but that O_2 had little additional benefit above a gaseous concentration of 1% at atmospheric pressure. Also, Janssen *et al.* (16) showed that ^{18}O was readily incorporated into the surface (and possibly subsurface by diffusion) of unsupported and various supported V_2O_5 catalysts during reaction with NO, NH_3, and $^{18}O_2$.

In the absence of gas-phase O_2, the NO–NH_3 reaction can lead to bulk reduction of the vanadia. Inomata *et al.* (10) showed that the vanadia was reduced after prolonged (60–70 min) reaction at 250°C in the absence of O_2 over initially oxidized V_2O_5. The average composition of the reduced vanadia was determined to be roughly V_2O_4 by estimating the amount of O removed as H_2O. The *ex situ* transmission IR spectra resembled those of V_2O_4, and *ex situ* EPR indicated the presence of V^{4+}.

Gas–Solid Reduction of a Metal Oxide

A general introduction to the gas–solid reduction of metal oxides can be found in the review by Koga and Harrison (19). Figure 2 shows the situation schematically. Initially the surface and bulk are fully oxidized. As the surface reduces and vacancies are formed, the subsurface layer reacts with vacancies at the surface to reoxidize the surface, leaving anion vacancies beneath the surface (Fig. 2a). As the surface continues to reduce, deeper layers must supply the oxygen to the surface. Vacancies diffuse deeper into the lattice while oxide anions move toward the surface (Fig. 2b). The oxide anions diffuse through the lattice by moving from

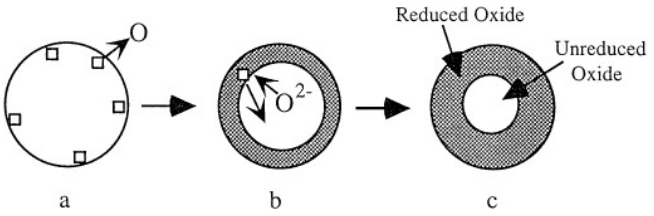

FIG. 2. Schematic diagram of gas–solid reduction of a metal oxide: (a) shortly after reduction begins; (b) formation of and subsequent propagation of the reduced phase by counter diffusion of anion vacancies (□) and oxide ions (O^{2-}); (c) continued propagation of the reduced phase into the unreduced core.

the current lattice position to an adjacent vacancy. The vacancies diffuse into the crystal lattice toward the core while the oxide anions diffuse out of the lattice toward the surface. At a sufficiently high density of lattice vacancies, the crystal structure becomes unstable. Thus, a new (reduced) crystalline phase will form by the local rearrangement of atoms to eliminate vacancies. As the surface gas–solid reduction continues, the reduced phase propagates further into the core of the oxide particle (Fig. 2c).

Many catalytic oxidation reactions over metal oxides may involve a balance between two sequential gas-solid reactions: reduction and reoxidation of the catalyst. Depending on the ratio of oxidizing and reducing agents in the gas phase, a net gas–solid reduction can result. The resulting change in metal valance state can change the kinetic behavior of the reaction. The present study focuses on the situation when the gas–solid reactions are not in balance for the $NO{-}NH_3$ reaction in the absence of O_2.

The transformation of the metal–oxygen stretching region of the IR spectrum is monitored *in situ* to provide a relative measure of the near-surface concentrations of V^{5+} and V^{4+} during the interactions of NH_3 and other reducing agents with V_2O_5 powder. IRES is also used to characterize the oxidation state of vanadium oxide *in situ* during the $NO{-}NH_3$ reaction in the absence of O_2. The mechanisms of the gas–solid reduction of vanadia with and without the presence of NO are compared.

EXPERIMENTAL

Apparatus

A detailed description of the *in situ*, flowthrough IR emission cell and flow system used in this study was presented previously (4, 20). A thin layer of catalyst powder (see Sample Preparation) was dispersed on a low-emissivity metal disk which is mounted on the heated sample stage (see Fig. 3). The sample is the source of IR radiation in the emission experiment; the IR source in the spectrometer is turned off and the source collection mirror removed for the emission experiments. Infrared radiation, which is emitted by the heated sample, is collimated by a paraboloidal collection mirror mounted above the cell. The collimated IR beam is directed into the Fourier transform infrared (FTIR) spectrometer (Mattson, Cygnus 100) where the spectrum is analyzed. The radiation emitted by the sample follows the normal source beam path to the mercury cadmium telluride (MCT) detector. A graybody sample, composed of a thick layer of V_2O_5 at the same temperature as the catalyst, was used to measure the background spectrum (4, 20).

The *in situ* IR cell and flow system described previously (4, 20) were modified for these studies in the following manner. A single 17-gauge (1/16-inch O.D.) No. 5 needle tube inserted so that the ~1-mm-diameter opening in the side of the tube is located directly above center of the sample was used to introduce the gas. A 0.020-inch, type-K thermocouple (Omega) was inserted to contact the sample disk near the center. A 0.75-inch-diameter-by-0.062-inch-thick solid-gold (99.99%) disk was employed to support the sample. The solid-gold disk provided the necessary low emissivity and did not oxidize under the conditions used in this study.

Helium (zero grade), ethylene (CP), oxygen (zero grade), nitric oxide (99%), and ammonia (anhydrous) were used without further purification. All experiments were run at atmospheric pressure.

The transmission IR spectrum was measured with the spectrometer in its normal configuration, i.e., the glow-bar source was on, and the source collection mirror was installed. The sample was mounted in the sample compartment using a magnetic sample holder (Mattson).

One vanadia sample was reduced with 100 cm^3 (STP)/min of 1% NH_3 (balance He) at 375°C for a period of >4 h to determine the degree of bulk reduction. The sample was reduced in a 6-mm-O.D. pyrex microreactor which is described elsewhere (20). Two methods of analysis were used:

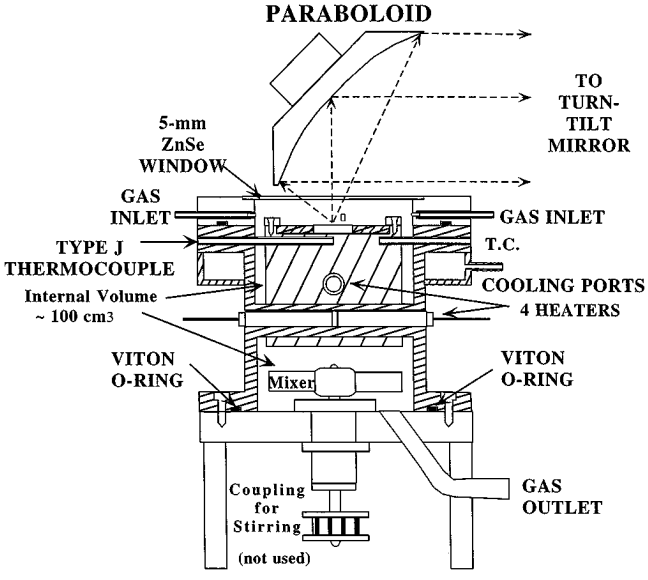

FIG. 3. A schematic of the custom *in situ* IRES cell and collection mirror. Not to scale.

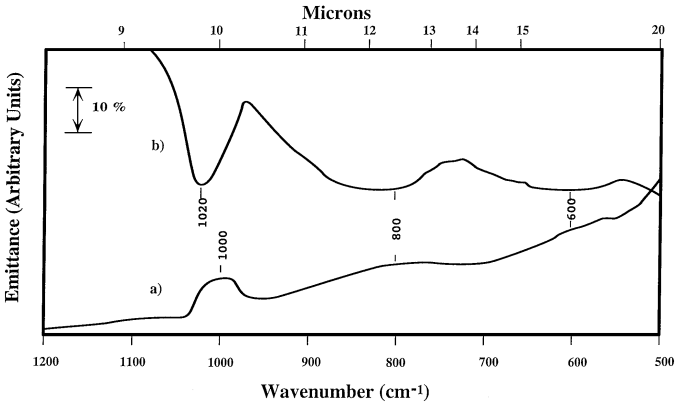

FIG. 4. The metal–oxygen stretching region of the IR spectrum for V_2O_5 powder: (a) Emission spectrum at 350°C; (b) transmission spectrum (1 wt.% in KBr).

vanadium analysis by atomic absorption spectroscopy, and temperature-programmed reoxidation with simultaneous thermal gravimetric analysis (TGA) and differential scanning calorimetry (DSC). The total mass of the sample in the microreactor after reduction was also compared to the mass of the initial loading. Vanadium analysis was performed by atomic absorption spectroscopy (Perkin–Elmer). A standard solution of vanadium pentoxide (Fisher) was used for the calibration. The temperature-programmed reoxidation of the sample was done with an STA 625 simultaneous thermal analyzer (Polymer Laboratories). The sample (10.429 mg) was heated to 200°C in flowing air at 30.0°C/min; then the rate was slowed to 5°C/min up to 575°C.

Sample Preparation

The emission (IRES) samples were prepared by spraying an ethanol slurry of the V_2O_5 powder (270/325 mesh) onto the gold disk. The loading was 0.2 to 0.5 mg/cm^2. A thicker sample (~0.8 mm), used to obtain the graybody reference spectra (20), was prepared by applying the slurry dropwise.

A transmission IR sample was prepared for comparison with the IRES spectra by pressing V_2O_5 powder (2% in KBr) into a wafer (~1 mm thick). The wafer was prepared by grinding and sieving V_2O_5 (Reagent Grade, Fisher) to 270/325 mesh and pressing the resultant powder mixed with KBr into a ~1-mm-thick disc. A transmission spectrum is only shown in Fig. 4b; all other spectra shown and analyzed are IRES spectra for bulk vanadia (no KBr).

Procedure

The preoxidized samples were treated in flowing O_2 (20%, balance He) at 400°C for at least 20 min prior to a reduction run. The sample was heated to the desired reduction temperature in flowing He. Once the sample reached thermal equilibrium, the spectrum of the preoxidized sample was recorded. Then the reactant gas flow was initiated and the IRES spectra were recorded automatically at predetermined time intervals.

Unless otherwise stated, a stoichiometric reaction feed refers to a flow consisting of 1.5% NO and 1.0% NH_3 (balance He).

Data Analysis

All emission spectra are displayed with the graybody representation as described previously (4, 20). All spectra consist of 128 scans at 8 cm^{-1} resolution. Spectral bands were integrated between two fixed wavenumbers. The baseline was taken as a straight line between the spectrum values at the endpoints of the integration region.

RESULTS

IR Emission Spectra

The metal–oxygen stretching regions of the IR emission (350°C) and transmission spectra of V_2O_5 are compared in Figs. 4a and 4b, respectively. Emission bands point above while transmission bands point below the baseline. Both spectra show a narrow band near 1000 cm^{-1} (1000 cm^{-1} for emission, 1020 cm^{-1} for transmission) and two broad bands at 800 and 600 cm^{-1}.

In situ IR emission spectra taken during hydrogen reduction of V_2O_5 at 280°C are shown in Fig. 5. The sample was preoxidized in 50 cm^3 (STP)/min of 20% O_2 (balance He) at 350°C overnight prior to reduction. Three strong bands are present in the initial spectrum. A broad band is centered at 800 cm^{-1}, and two narrower bands are located at 910 and 1000 cm^{-1}. A weaker band is also present at 950 cm^{-1}.

As the reduction with hydrogen proceeds, the intensity of the band at 910 cm^{-1} increases, becoming the dominant feature after 40 min. The intensity of the 1000-cm^{-1} band and the broad band at 800 cm^{-1} both decrease. The 800 and 1000-cm^{-1} bands both split into two narrower bands (720 and 830 cm^{-1} from the 800-cm^{-1} band, and 970 and

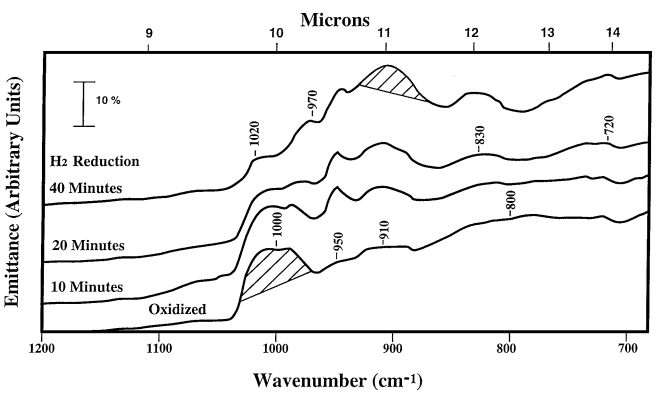

FIG. 5. The *in situ* IRES spectra of V_2O_5 during reduction with H_2 (100 cm^3 (STP)/min) at 280°C.

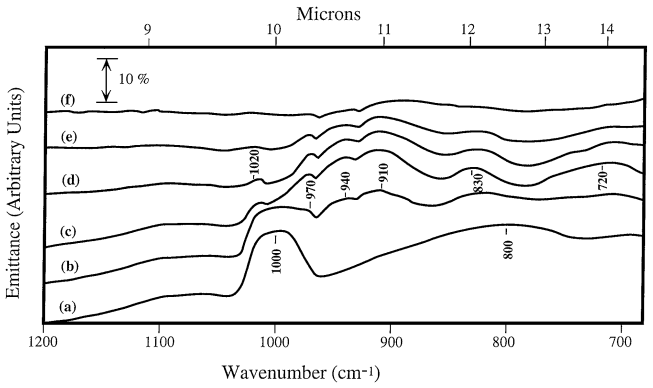

FIG. 6. The *in situ* IRES spectra of V_2O_5 during reduction in ammonia (2%, balance He) at 350°C: (a) initial spectrum; after (b) 10 min; (c) 20 min; (d) 60 min; (e) 120 min; (f) 600 min.

1020 cm^{-1} from the 1000-cm^{-1} band) after 20 min. In both cases, as reduction proceeds, the new bands shift away from each other and the original parent peak location. The weak feature at 950 cm^{-1} initially increases but then decreases after 20 min. Similar results have been obtained from reduction with ethylene (20).

Reduction with ammonia (2% in He) proceeds in a manner analogous to hydrogen as shown in Fig. 6. The two initial bands (800 and 1000 cm^{-1}) decrease, and each splits into two new bands (720 and 830 cm^{-1} from the 800 cm^{-1} band, 970 and 1020 cm^{-1} from the 1000-cm^{-1} band). Two new bands appear (910 and 940 cm^{-1}) after a few minutes, increase to a maximum, and then decrease.

The oxidation process mimics the reduction process in reverse. The reversibility of the reduction process can be seen in the typical series of spectra taken during the oxidation with oxygen (10% in He, 100 cm^3 (STP)/min) at 350°C of a reduced sample in Fig. 7. Initially no strong bands are present in the spectrum. After 60 min, a strong band appears at 1000 cm^{-1}, and several weak bands appear at 750, 820, and 910 cm^{-1}. The 1000-cm^{-1} band increases monotonically and approaches a steady-state intensity. The 750- and 820-cm^{-1} bands increase and merge to form a broad steady-state band centered at 800 cm^{-1}. The 910-cm^{-1} band increases to a maximum intensity (~60 min) and then decreases. Eventually, it disappears.

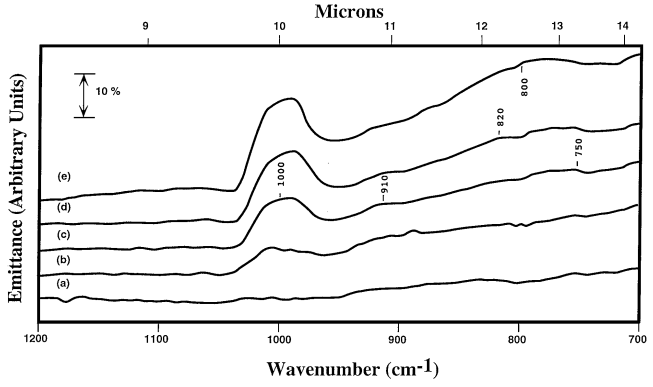

FIG. 7. The *in situ* IRES spectra of ethylene-reduced V_2O_5 during reoxidation with O_2 (10% balance He, 100 cm^3 (STP)/min) at 300°C: (a) initial spectrum; after (b) 60 min; (c) 120 min; (d) 180 min; (e) 240 min.

Integrated Band Intensities—Reduction

Integrated areas of the 1000-cm^{-1} band (970–1030 cm^{-1}) and the 910-cm^{-1} band (870–930 cm^{-1}) for ethylene (10% in He) and ammonia (2.5% in He) reduction at various temperatures are shown in Figs. 8 and 9, respectively. In both cases, the 1000-cm^{-1} band decreases monotonically, and the 910-cm^{-1} band intensity increases, goes through a maximum, then decreases. Both the 1000- and 910-cm^{-1} bands generally approach zero at long times. However, in two of the low-temperature runs (ethylene at 300°C and ammonia at 250°C), the 910-cm^{-1} band did not reach its maximum value before the experiment was stopped.

A sharp change in the slope of the 1000-cm^{-1} band data for reduction by ethylene (Fig. 8a) occurs when the area reaches about 1.25 (arbitrary units) for temperatures above 300°C. The transition corresponds to a point when the 910-cm^{-1} band reaches 60–80% of its maximum area.

As temperature decreases, the reduction time increases dramatically. Initial reduction rates can be calculated from the slope of the 1000-cm^{-1} band curves in Figs. 8a and 9a. An Arrhenius plot for initial rates calculated from the

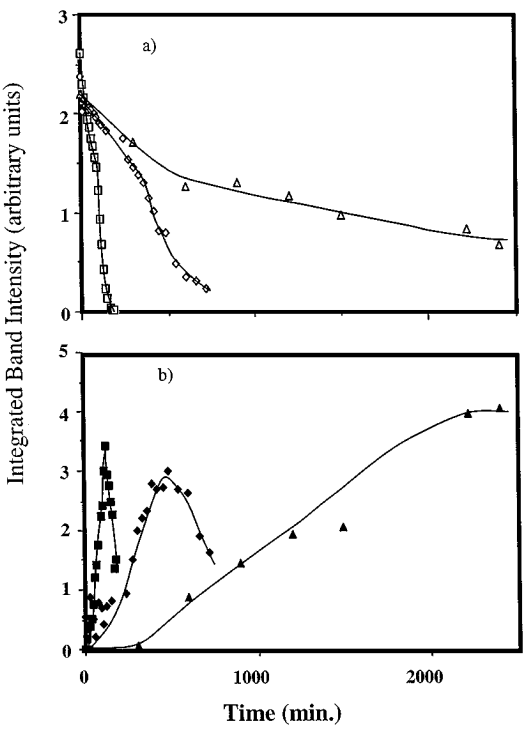

FIG. 8. Integrated intensities of the (a) 1000-cm^{-1} band (970–1030 cm^{-1}) and (b) 910-cm^{-1} band (870–930 cm^{-1}) during ethylene reduction at 300°C (△, ▲), 325°C (◇, ◆), and 350°C (□, ■).

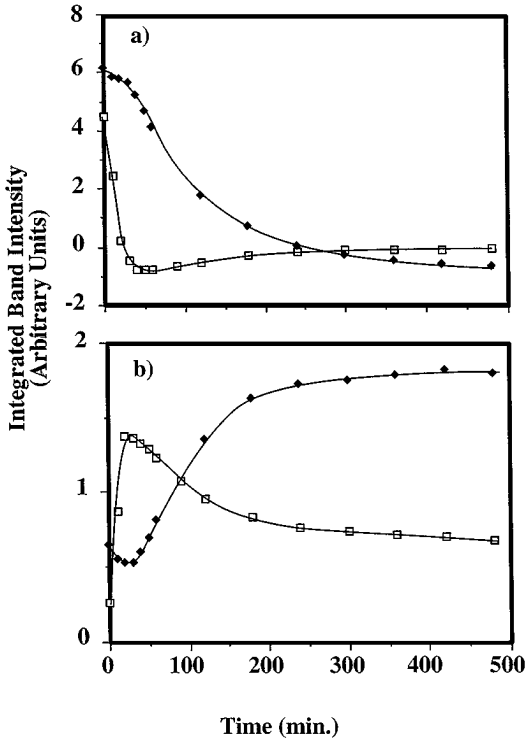

FIG. 9. Integrated intensities of the (a) 1000-cm^{-1} band (970–1030 cm^{-1}) and (b) 910-cm^{-1} band (870–930 cm^{-1}) during ammonia reduction at 250°C (◆) and 300°C (□).

ethylene-reduction data is shown in Fig. 10. The apparent activation energy is 180 kJ/mol (43 kcal/mol). The apparent activation energy for ammonia reduction (134 kJ/mol), based on the two temperatures that were tested, is similar to that for ethylene reduction.

Integrated Band Intensities—Oxidation

Integrated areas of the 1000-cm^{-1} band (970–1030 cm^{-1}) and the 910-cm^{-1} band (870–930 cm^{-1}) for oxidation with oxygen (10% in He) of ethylene-reduced vanadia at various

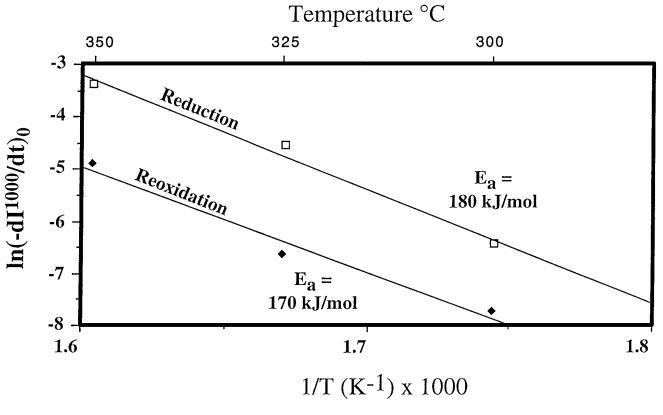

FIG. 10. Arrhenius plot of initial rates of reduction (□) with ethylene and reoxidation with O_2 (◆).

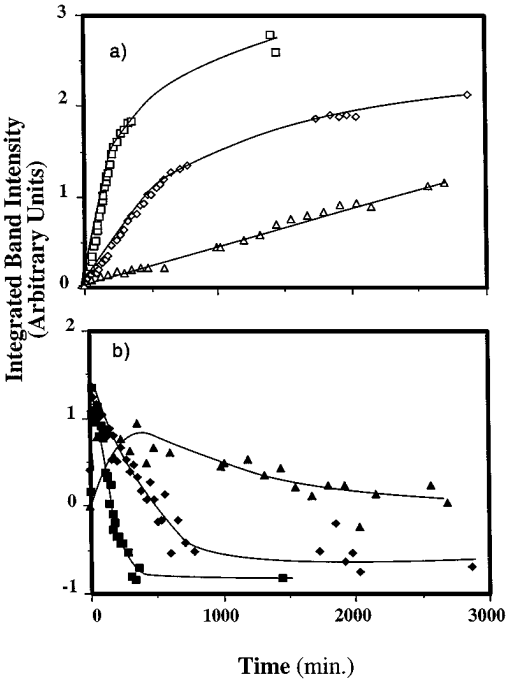

FIG. 11. Integrated intensities of the (a) 1000-cm^{-1} band (970–1030 cm^{-1}) and (b) 910-cm^{-1} band (870–930 cm^{-1}) during reoxidation of ethylene-reduced V_2O_5 at 300°C (△, ▲), 325°C (◇, ◆), and 350°C (□, ■).

temperatures are shown in Fig. 11. The 1000-cm^{-1} band increases continuously to a steady-state value, while the 910-cm^{-1} band increases to a maximum and then decreases to zero.

The apparent oxidation rate also depends strongly on temperature. The activation energy (Fig. 10b) for oxidation is 170 kJ/mol (41 kcal/mol) based on the initial rate of increase of the 1000-cm^{-1} band. This is close to the value found for reduction with ethylene and ammonia.

IR Emission Spectra—NO–NH_3 Reaction

The bulk reduction of V_2O_5 during the reaction of NO and NH_3 on the surface at 315°C is characterized by the series of *in situ* IR emission spectra shown in Fig. 12. The spectrum of the initially oxidized V_2O_5 (2.5% NO, Balance He, Fig. 12a) is characterized by a narrow band at 1000 cm^{-1} and a broader band centered at 800 cm^{-1}. As the reaction proceeds, the spectrum evolves in a manner analogous to the bulk reduction of V_2O_5 with ammonia alone (see Fig. 6). The two initial bands (800 and 1000 cm^{-1}) decrease (Fig. 12b), and each splits into two new bands (710 and 830 cm^{-1} from the 800-cm^{-1} band, and 970 and 1020 cm^{-1} from the 1000-cm^{-1} band; see Figs. 12c and 12d). Two new bands appear (910 and 950 cm^{-1}) after 30 min (Fig. 12b) and the intensities increase as the vanadia reduction proceeds (Figs. 12d and 12e).

Integrated areas of the 1000- and 910-cm^{-1} bands for a stoichiometric feed of NO and NH_3 at 315, 325, and

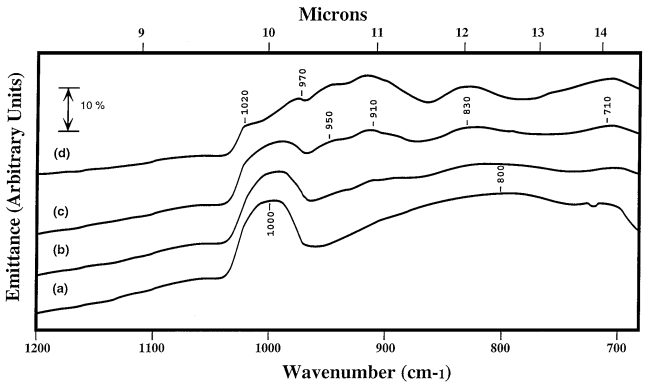

FIG. 12. The *in situ* IRES spectra of V_2O_5 powder during the surface reaction between NO (1.5%) and NH_3 (1.0%, balance He) at 315°C: (a) initial spectrum; after (b) 30 min; (c) 60 min; (d) 120 min.

350°C are shown in Fig. 13. The total flow rate was 400 cm^3 (STP)/min at 350°C, and 100 cm^3 (STP)/min at 315 and 325°C. In each case, the 1000-cm^{-1} band decreases monotonically while the 910-cm^{-1} band increases to a maximum. At longer times, the 910-cm^{-1} band decreases again.

The rate of reduction is a strong function of temperature. The time for the 1000-cm^{-1} curve to reach steady state (reduction time) varies by an order of magnitude from 315 to 350°C. The initial rates of reduction, as estimated from the initial slope of the 1000-cm^{-1} band data, were used to construct the Arrhenius plot in Fig. 14. The apparent activation energy is 206 kJ/mol (49 kcal/mol).

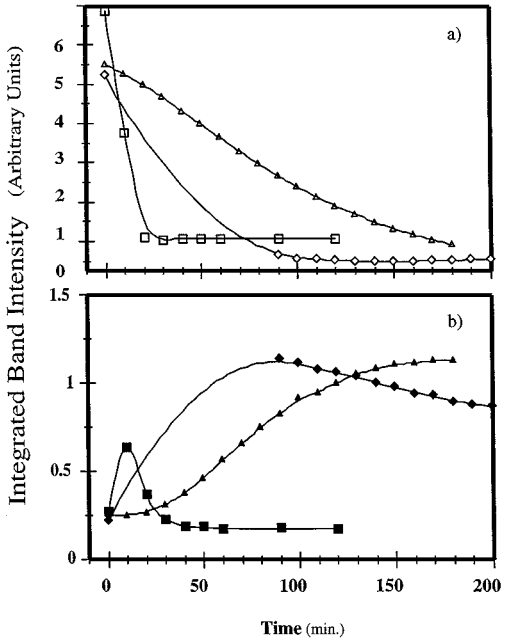

FIG. 13. Integrated intensities of the (a) 1000-cm^{-1} band (970–1030 cm^{-1}) and (b) 910-cm^{-1} band (870–930 cm^{-1}) during the NO–NH_3 reaction at 315°C (△, ▲), 325°C (◇, ◆), and 350°C (□, ■).

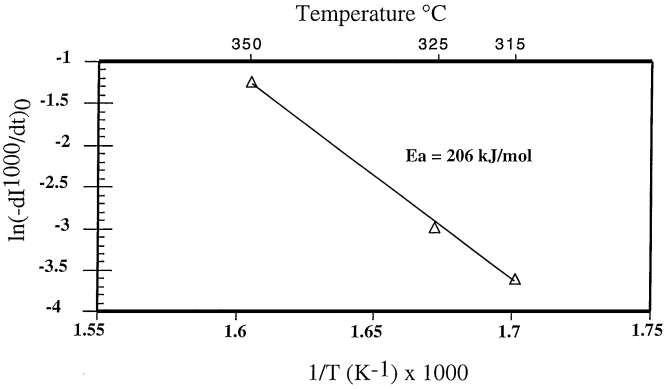

FIG. 14. Arrhenius plot of the initial rate of reduction of V_2O_5 during the NO–NH_3 reaction.

Sample Analysis

The mass loss from the total catalyst charge removed from the microreactor following NH_3 reduction at 375°C corresponded to 49% reduction from V_2O_5 to V_2O_3 (i.e., an average composition of V_2O_4). The V analysis results for the reduced vanadia sample (Table 1) indicate 51.7% reduction, while mass increase (18%) during temperature-programmed reoxidation corresponds to 47% reduction from V_2O_5 to V_2O_3. The total heat evolved was 13.1 kcal/mol at ~336°C, which is similar to the value reported for ΔH_{636K} for the oxidation of V_2O_4 to V_2O_5 (−18 kcal/mol) (21).

DISCUSSION

The infrared emission spectrum provides valuable insight into the mechanism of the solid-state reduction of V_2O_5. Figures 5 and 6 show the transformations in the metal–oxygen stretching region of the emission spectra during V_2O_5 reduction with two different reducing agents. The surface is reduced first. As reduction proceeds, oxygen atoms are removed from the bulk of the crystal lattice. Initially, the crystal structure may remain intact, though with an increasing number of oxygen vacancies. Eventually the atoms rearrange, eliminating may of the vacancies and forming a new crystal structure. The frequency of the V–O stretch is sensitive to changes in the vanadium oxide structure.

The spectrum of V_2O_5 (Fig. 4) contains three strong features which correspond to different types of V–O bonds

TABLE 1

Vanadium Analysis Results of Vanadia after Reduction in Ammonia at 375°C

V% (wt/wt)	O% (wt/wt)	O/V (g/g)	O/V (mol/mol)	Percent reduction (V_2O_3 = 100%)
61.6	38.4	0.623	1.99	51.7

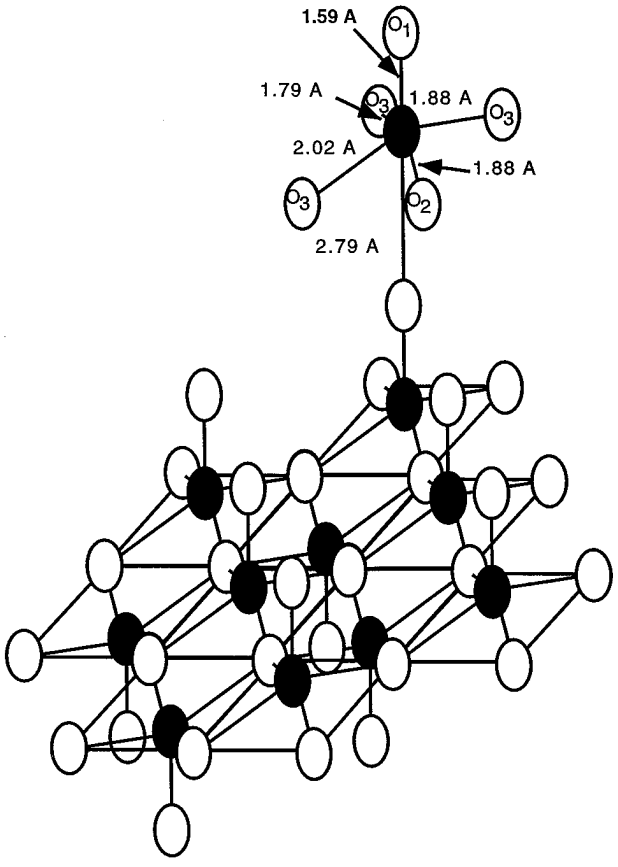

FIG. 15. The structure of V_2O_5 showing layers parallel to the (010) plane (after Bielanski (18)).

in the V_2O_5 crystal lattice. The structure of V_2O_5 can be represented by a distorted square-based pyramid (Fig. 15) (18, 22, 23). Vanadium (closed circles) is located inside of the polyhedron with the oxygen (open circles) atoms at the vertices. The bases of the pyramids are connected by a combination of shared corners and edges to form layers parallel to the (010) plane with the apices of the pyramids perpendicular to the layers. A weak coordination bond (2.79 Å) between the layers completes the coordination of six. The shortest V−O bond (1.54 Å), which forms the apex of the pyramid, is between vanadium and terminally bonded oxygen. This bond has significant double bond character and is characterized by an IR band at 1020 cm^{-1} (22, 24). The four remaining oxygen atoms make up the layer. Three of these (labeled O_3) are bonded to three vanadium atoms while the fourth (O_2) is bonded to two vanadium atoms. These O−V−O stretches are characterized by the IR bands at about 820 and 600 cm^{-1} (22, 23).

Upon mild reduction with H_2, or NH_3, the V_2O_5 spectral features are replaced by new features dominated by a strong band at 910 cm^{-1} (Figs. 5 and 6). This spectrum strongly resembles the IR spectrum of V_2O_4 (25).

The 910-cm^{-1} band is most likely due to the O−V^{4+}−O stretch (23, 25). The 1020-cm^{-1} band is absent from the spectrum of V_2O_4 since there is no terminal oxygen in the V_2O_4 crystal structure. Upon further reduction, only weak features are present in the IR spectrum (Fig. 6), which is consistent with the IR spectrum of V_2O_3 (25). Further reduction to lower vanadium oxides is not expected in this temperature range (<900°C) (26).

Considering the above assignments, the 1020- and the 910-cm^{-1} band curves represent a near-surface measure of V^{5+} content (in the V_2O_5 structure) and V^{4+} content (in a V_2O_4 structure), respectively. From these curves, it is apparent that oxidation and reduction occur stepwise, i.e., $V^{5+} \rightarrow V^{4+} \rightarrow V^{3+}$. During reduction (e.g., Fig. 8), the V^{5+} signal decreases monotonically as the V^{5+} is initially converted to V^{4+} (indicated by the initial increase in the V^{4+} IR signal). The V^{4+} signal goes through a maximum and then decreases as V^{4+} is converted to V^{3+}. The V^{3+} content, if it were measured, would rise in a sigmoidal fashion to a steady-state value corresponding to complete reduction. Oxidation occurs by the reverse process (Fig. 11). The V^{5+} signal resembles the hypothetical V^{3+} curve described above for reduction, while a hypothetical V^{3+} curve for oxidation would resemble the V^{5+} curve observed for reduction. The V^{4+} signal behaves similarly for both oxidation and reduction.

Additional evidence for stepwise reduction was obtained by Bielanski *et al.* (3) from *ex situ* electron paramagnetic resonance studies of V_2O_5 reduction with propylene. Curves of V^{4+} content were reported as a function of exposure time. Those curves are very similar to the curves obtained in this study by *in situ* emission IR. Similarly, Bosch *et al.* (26) observed a stepwise reduction during hydrogen temperature-programmed reduction (TPR) of bulk V_2O_5. Depending on the heating rate, as many as four major TPR peaks were observed. Additional unresolved peaks were also apparent. Samples from each of the major TPR peaks were quenched in N_2 and analyzed by X-ray diffraction and thermal gravimetric analysis in air. Both techniques confirmed that reduction occurred in a stepwise fashion.

The activation energies observed for oxidation and reduction (170 and 180 kJ/mol, respectively) are quite high. Similar activation energies were observed for reduction of V_2O_5 by propylene (3) and hydrogen (26) (126 and 200 kJ/mol, respectively).

These apparent activation energies for reduction and oxidation are higher than would be expected if the surface reaction were rate controlling. Typical values of activation energy for the latter process are less than 30 kJ/mol (3, 27). These high activation energies are, however, typical of solid-state lattice diffusion (28). Unlike gas- and liquid-phase diffusion, solid-state diffusion by vacancy motion is an activated process with a high apparent activation energy. The atoms have to overcome the potential barrier from changes in association with the surrounding atoms in order to pass from one lattice site to another. The activation

energy for lattice diffusion is typically very large (100–300 kJ/mol) while the diffusivity is typically very low (10^{-10} cm^2/s or less for a polycrystalline material at room temperature) (28). Samsonov (29) reports the activation energy of 255 kJ/mol for the diffusivity of oxygen through the lattice of an annealed single crystal of V_2O_5 in the temperature range 560–650°C. Extrapolating these data, the diffusivity at 350°C is estimated to be $\sim 10^{-17}$ cm^2/s. The greater number of vacancies and defects in polycrystalline V_2O_5 greatly facilitates diffusion. The defects result in an effective diffusivity which is several orders of magnitude higher and an activation energy which is lower than observed for a low defect single crystal (28).

The diffusivity can also be estimated from the characteristic diffusion length and corresponding diffusion time. Using the particle radius (25 μm) and the time for complete oxidation (from Fig. 13, ~1500 min at 350°C) the difussivity is estimated to be 10^{-10} cm^2/s, which is a reasonable value for solid-state diffusion in a polycrystalline material (28).

If the gas–solid reaction at the surface of the oxide is sufficiently fast, solid-state diffusion may control the overall rate of reduction. A classic result for a diffusion-controlled process in a semi-infinite medium is that the increase in the total amount of diffusing material (oxygen atoms) will scale with $\sqrt{t}$ (e.g., Crank (30)). Figure 16 demonstrates this result for the V^{4+} IR signal during oxidation at 325 and 350°C. The V^{5+} signal during oxidation, as well as both V^{4+} and V^{5+} signals for reduction, exhibits, similar behavior.

The IR data (Figs. 12 and 13) demonstrate that NO–NH_3 mixtures, in spite of a large excess of NO (up to 100 : 1 (20)), result in a net reduction of V_2O_5. This result is surprising considering NO is quite capable of oxidizing vanadia. This capability was demonstrated by the fact that the sample used to obtain the data in Figs. 12 and 13 was reoxidized, in each case, with NO (1–2.5%). The result confirms earlier reports (9, 10, 12, 14, 31) that NH_3 is adsorbed more strongly than NO. Ammonia aparently blocks sites for NO adsorption, preventing it from reoxidizing the surface. This explanation is consistent with an Eley–Rideal mechanism,

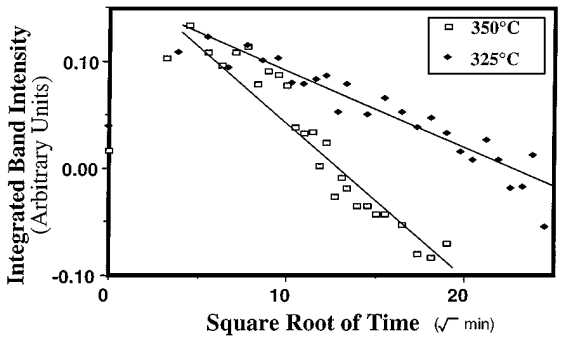

FIG. 16. Plot showing that the 910-cm^{-1} IRES band (for V^{+4}) scales linearly with the square root of time during the oxidation of reduced vanadia by O_2 at 325 and 350°C.

as has been proposed for the catalytic reduction of NO on vanadia (7, 9–11, 16, 32). NO reacts with NH_3 from the gas phase or a weakly bonded surface state, but it cannot react with the reduced surface to any great extent when NH_3 is present. In contrast to NO, O_2 can react with the vanadia surface during the NO–NH_3 reaction as noted earlier (10, 16). Gaseous O_2 maintains the oxidation state of the vanadia, while in the absence of O_2, the vanadia reduces as observed in the present study.

The time required to reduce the sample with a stoichiometric NO–NH_3 mixture is significantly greater than for NH_3 alone. For example, at 315°C, about 200 min is required for the 1000-cm^{-1} band to disappear with the stoichiometric feed (Fig. 12), compared to 30 min at 300°C for NH_3 alone (see Fig. 9). While the NH_3 reduction data were obtained for a higher NH_3 level (2.5% vs 1.0%), the presence of NO clearly affects the reduction rate. Apparently, some NO was adsorbing and reoxidizing a few vanadia sites; however, the surface was predominantly covered with NH_3, so net reduction of the vanadia occurred.

Other than the rate, reduction with NO–NH_3 mixtures appears to occur in exactly the same fashion as for a simple reductant such as ammonia or hydrogen. V^{5+} (indicated by the 1000-cm^{-1} band) is reduced to V^{4+} (indicated by the 910-cm^{-1} band), which is subsequently reduced to V^{3+} (not detected with IR) in a stepwise fashion. The high activation energy (206 kJ/mol; see Fig. 14) suggests that solid-state diffusion also controls the rate of vanadia reduction during the NO–NH_3 reaction.

Both the vanadium analysis and reoxidation results indicate that as a result of NH_3 reduction at 375°C, the vanadia was reduced about 50% from V_2O_5 to V_2O_3; i.e., the vanadia had the average composition V_2O_4. The IR data indicates that even at lower temperatures, the near-surface region is primarily V_2O_3. This suggests that the vanadia particles are more reduced near the surface and are increasingly more oxidized deeper into the particles.

The fact that the vanadia was not completely reduced, even though the NH_3 conversion had become immeasurable, suggests that the reduction either stopped or became imperceptibly slow. The latter seems more likely. Perhaps the remaining oxygen atoms are in areas of low defect density, so that the diffusivity approaches that of a single crystal, which may be orders of magnitude smaller than the effective polycrystalline diffusivity.

The sharp change in the rate of decrease of the V^{5+} IR signal during reduction with ethylene (Fig. 8) indicates an abrupt change in the mechanism which controls this rate. The transition consistently occurs at approximately the same degree of bulk reduction (as indicated by the ordinate value in Fig. 8). It seems likely that the new process is occurring in the bulk of the solid rather than at the surface since the reduction rate is controlled by oxygen diffusion through the bulk.

The IR signal at 1000 cm^{-1} is specifically detecting terminal oxygen atoms bonded to V^{5+} within the V_2O_5 crystalline structure. Therefore this signal intensity decreases via the following mechanism. Oxygen is removed from the surface via reduction by the gas phase. The resulting oxygen vacancy at the surface can diffuse back into the lattice, and lattice oxygen from the bulk can diffuse to the surface. The net result is that lattice oxygen is replaced by vacancies. As the defect density (primarily vacancies) continues to increase, the V_2O_5 structure becomes unstable and thus rearranges to eliminate defects. A reduced phase (e.g., V_2O_4) is formed which does not contain V=O (33). This rearrangement results in the loss of the V^{5+}-signal intensity.

The structural rearrangement can occur by the same vacancy-diffusion mechanism as the transport of oxygen to the surface. This mechanism probably results in the initial rate of decrease in the 1000-cm^{-1} band intensity at a rate comparable to the oxygen transport mechanism. The dramatic acceleration in the rate of decrease of the 1000-cm^{-1} band intensity suggests that a transition to a much faster mechanism is responsible.

Faster mechanisms for structural rearrangement are known to occur (28) in crystalline solids when defects tend to be located preferentially within a single plane (known as a slip or shear plane). As the name suggests, these shear planes can slide along one another in order to eliminate a large number of defects in a concerted manner. Vanadia is known to exhibit a homogenous series of phases with the general formula, V_nO_{2n-1} ($n = 4$–8), which is due to the periodic ordering of shear planes (or Magnéli defects) (21, 29). Several of these phases were observed by Bosch *et al.* (26) during hydrogen TPR of bulk V_2O_5. This may explain the fast rearrangement evidenced in Fig. 3.7a.

While the overall rate of reduction appears to be limited by solid-state mechanisms, the surface chemistry is still important. This is clear from the fact that the reduction occurs much more quickly with ammonia than with ethylene as the reducing agent. While ammonia tends to adsorb on acid sites (both Brønsted and Lewis (14, 34)), ethylene probably adsorbs on the cation sites with its π electrons overlapping the empty *d* orbitals in vanadium (18). This difference probably leads to different mechanisms for the surface reactions involving the two reducing agents, which may explain the difference in the reduction rates.

CONCLUSIONS

The metal–oxygen stretch region of the IR emission spectrum of V_2O_5 is shown to provide a means of characterizing the relative amounts of V^{5+} and V^{4+} near the surface of the sample. *In situ* spectra obtained during reduction of V_2O_5 with hydrogen, ethylene, or ammonia, and subsequent reoxidation with oxygen, provided valuable insight into the solid-state mechanisms which control the rate of the reaction.

This study suggests that net changes in the structure and metal valence state of a metal-oxide catalyst can occur during a catalytic oxidation/reduction process. These changes may in turn have a profound effect on the catalytic properties of the oxide.

NO–NH_3 mixtures were shown to cause a net reduction of V_2O_5 powder even with a large excess of NO. The reduction occurs in the same manner as seen for V_2O_5 reduction with simple reductants (hydrogen, ethylene, and ammonia), i.e., stepwise reduction of vanadium ($V^{5+} \rightarrow V^{4+} \rightarrow V^{3+}$) with solid-state diffusion of O atoms as the rate-limiting process. There is no evidence from these *in situ* IRES studies for reduction of V^{5+} directly to V^{3+}.

It should be noted that these studies may only indirectly relate to supported vanadia-based SCR catalysts. Specifically, the preferred supports (e.g., titania) may modify the solid-state redox mechanisms and kinetics that we have found. These studies provide an *in situ* perspective by which the influence of the support may be understood.

ACKNOWLEDGMENT

We thank the Department of Energy, Office of Basic Energy Sciences (Grant DE-FG02-87ER13772) for financial support of this work.

REFERENCES

1. Centi, G., Fornasari, G., and Trifirò, F., *J. Catal.* **89**, 44 (1984).
2. Lunsford, J., *in* "Catalysis: Science and Technology" (J. Anderson and M. Boudart, Eds.), Springer-Verlag, New York, Vol. 8, pp. 227–256, 1987.
3. Bielanski, A., Dyrek, K., and Serwicka, E., *J. Catal.* **66**, 316 (1980).
4. Sullivan, D. H., Conner, W. C., and Harold, M. P., *Appl. Spectrosc.* **46**, 811 (1992).
5. Musikant, S., "Optical Materials: An Introduction to Selection and Application," Dekker, New York, 1985.
6. Flagan, R. C., and Seinfeld, J. H., "Fundamentals of Air Polution Engineering," Prentice Hall, Englewood Cliffs, NJ, 1988.
7. Bosch, H., and Janssen, F. J. J. G., *Catal. Today* **2**, 369 (1988).
8. Wood, S. C., *Chem. Eng. Prog.* **90**, 32 (1994).
9. Miyamoto, A., Inomata, M., Yamazaki, Y., and Murakami, Y., *J. Catal.* **57**, 526 (1979).
10. Inomata, M., Miyamoto, A., and Murakami, Y., *J. Catal.* **62**, 140 (1980).
11. Miyamoto, A., Yamazaki, Y., Inomata, M., and Murakami, Y., *J. Phys. Chem.* **85**, 2366 (1981).
12. Miyamoto, A., Kobayashi, K., Inomata, M., and Murakami, Y., *J. Phys. Chem.* **86**, 2945 (1982).
13. Miyamoto, A., Yamazaki, Y., Hattori, T., Inomata, M., and Murakami, Y., *J. Catal.* **74**, 144 (1982).
14. Topsøe, N.-Y., *J. Catal.* **128**, 499 (1991).
15. Sobalik, Z., Pour, V., Sokolova, L. A., Nevskaya, O. V., and Popova, N. M., *Collect. Czech. Chem. Commun.* **50**, 1259 (1985).
16. Janssen, F. J. J. G., van den Kerkhof, F. M. G., Bosch, H., and Ross, J. R. H., *J. Phys. Chem.* **91**, 5921 (1987).
17. Ozkan, U. S., Cal, Y., Kumthekar, M. W., and Zhang, L., *J. Catal.* **142**, 182 (1993).
18. Bielanski, A., and Haber, J., "Oxygen in Catalysis," 1st ed., Vol. 43. Dekker, New York, 1991.

19. Koga, Y., and Harrison, L. G. (Eds.), "Reactions of Solids with Gases Other Than Oxygen," 1st ed., Vol. 21, p. 119. Elsevier, New York, 1984.
20. Sullivan, D. H., "Solid-State Catalyst Transformations during Oxidation Reactions over Vanadium Oxide." Ph.D. Thesis, University of Massachusetts, 1994.
21. Trotman-Dickenson, A. F. (Eds.), "Comprehensive Inorganic Chemistry." Pergamon, New York, 1973.
22. Kera, Y., and Hirota, K., *J. Phys. Chem.* **73**, 3973 (1969).
23. Primet, M., Fouilloux, P., and Imelik, B., *Surf. Sci.* **85**, 457 (1979).
24. Barraclough, C. G., Lewis, J., and Nyholm, R. S., *J. Chem. Soc.*, 3552 (1959).
25. Frederickson, L. D., and Hausen, D. M., *Anal. Chem.* **35**, 818 (1963).
26. Bosch, H., Kip, B. J., van Ommen, J. G., and Gellings, P. J., *J. Chem. Soc. Faraday Trans. 1* **80**, 2479 (1984).
27. Coulson, D. R., Mills, P. L., Kourtakis, K., Lerou, J. J., and Manzer, L. E. (Eds.), "Kinetics of me Reoxidation of Propylene-Reduced γ-Bismuth Molybdate: A TAP Reactor Study," 1st ed., Vol. 72, p. 305. Elsevier, New York, 1992.
28. Wert, C. A., and Tompson, R. M., "Physics of Solids," 2nd ed. McGraw–Hill, New York, 1970.
29. Samsonov, G. V., "The Oxide Handbook," 1st ed. IFI/Plenum, New York, 1982.
30. Crank, J., "The Mathematics of Diffusion." Oxford Univ. Press, Oxford, 1975.
31. Smak, T. Z., Dumesic, J. A., Clausen, B. S., Tomqvist, E., and Topsøe, N.-Y., *J. Catal.* **135**, 246 (1992).
32. Janssen, F. J. J. G., van den Kerkhof, F. M. G., Bosch, H., and Ross, J. R. H., *J. Phys. Chem.* **91**, 6633 (1987).
33. Wychoff, R. W., "Crystal Structures," Vol. 2. Interscience, New York, 1964.
34. Belokopytov, Y. V., Kholyavenko, K. M., and Gerei, S. V., *J. Catal.* **60**, 1 (1979).